Application of a Rapid Design Tool to a 3D Woven Structural Joint

Evgenia Plaka[1] and Stephen P. Jones[2]
University of Massachusetts Lowell, Lowell, MA, 01854, USA

Brett A. Bednarcyk[3] and Evan J. Pineda[4]
NASA Glenn Research Center, Cleveland, OH, 44135, USA

Richard Li[5]
Aurora Flight Sciences, A Boeing Company, Cambridge, MA, 02140, USA

Marianna Maiaru[6]
University of Massachusetts Lowell, Lowell, MA, 01854, USA

The optimization of composite structural joints is an iterative process and a multiscale problem. High fidelity finite element modeling of joints with 3D woven and laminated materials can become computationally expensive. The aim of this paper is to establish a reliable analysis process for the optimization of a composite Y-joint (curved Pi-joint), to be used in an aircraft fuselage, using commercial rapid joint design, analysis, and optimization software. The rapid joint design tool was investigated as a substitute and/or complement to a finite element analysis software. A composite Pi-joint and a composite Y-joint were evaluated using the rapid joint design tool to determine the applicability and limits of the software. Furthermore, three main preliminary parametric studies were performed to better understand the capability of the tool in predicting the stress distributions and trends in the Y-joint. The parameters investigated were the joint curvature, the laminated skin thickness, the adhesive systems, and the ply composition. Lastly, trends in predicted failure load were produced as a function of skin thickness (16ply, 24ply and 32ply). Failure loads were found with varying joint curvature and skin thickness using stress-based adherend failure criterion. The rapid joint design tool was also validated against existing experimental results.

I. Introduction

Fiber reinforced polymer composites (FRPCs) are widely used in the aerospace industry due to their high specific strength and stiffness. While unidirectional FRPCs have been preferred in the past and have a range of applications, there has been an increase in the production and use of 3D woven composite materials. One of the main additional advantages in using 3D woven composites is the enhanced through-thickness properties [1], [2], which are favorable in applications with significant out-of-plane loading, such as structural joints in aircrafts. Due to the complex architecture of 3D woven polymer composites, their behavior is not yet fully characterized and understood across the length scales (nanoscale through macroscale). Consequently, parts using these materials are often overdesigned,

[1] Graduate Student, Department of Mechanical Engineering, AIAA Member.
[2] Aerospace Structural Engineer, AIAA Member.
[3] Materials Research Engineer, AIAA Associate Fellow.
[4] Aerospace Research Engineer, AIAA Senior Member.
[5] Structures Research Engineer, AIAA Member.
[6] Assistant Professor, Department of Mechanical Engineering, AIAA Member.

yielding higher costs and weight in the structures. In efforts to optimize a composite structure, it is key to understand the behavior and cause of failure of composite materials. The composite structures may contain many degrees of freedom and many loading cases, requiring high computational analysis time. Hence, design tools based on lower fidelity models and more rapid analysis are usually considered as a preliminary step in the characterization process. More significantly, rapid design tools can give useful information through parametric studies that provide insight on trends.

The focus is the study of a composite structural Y-joint proposed to be used in the D8 Double Bubble aircraft, a concept born during the NASA N+3 study [3] - [5]. The current design calls for a structural joint made of a 3D woven composite preform material and unidirectional FRPC skin. According to experimental tests from Aurora Flight Sciences, A Boeing Company (Aurora) [4], the current Y-joint design consistently failed in the joint center region close to the preform-to-skin interface, see Fig. 1.

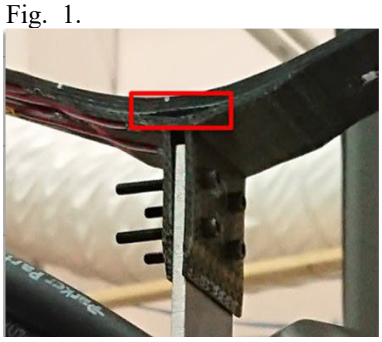

Fig. 1 Initial failure region in the Y-joint as seen in experiments [4].

This paper explores the use of rapid analysis software as a substitute and/or complement to finite element analysis software, for the analysis of this D8 Double Bubble Y-joint. The Y-joint was first analyzed with commercial finite element software, Abaqus, and secondly in the commercial HyperX structural analysis/sizing software [6]. Two composite joints were evaluated: a more common Pi joint and a Y-joint (curved Pi). Both joints represent new applications for the HyperX bonded joint analysis, as the software does not explicitly include a Pi-joint capability, nor the ability to consider initially curved geometries (like the Y-joint). As such, the Pi joint has been decomposed into two simpler joints for analysis in HyperX, and the effects of the initial curvature have been incorporated through the application of appropriate boundary conditions. Results show the comparisons and agreement between finite element and HyperX results, demonstrating HyperX as a viable solution for rapid analysis of these joint configurations. Furthermore, three parametric studies were conducted in HyperX. Two more Y-joints with different curvatures were modeled to evaluate the impact of degree of curvature of the joint performance. In addition, the effects of skin thickness (which constitutes one of the joint adherends) was investigated by comparing a 16 ply, 24 ply, and 32 ply laminated skin. Finally, two types of adhesive systems (film adhesives and paste adhesives) were explored. Failure loads for the cases of varying curvatures and skin thicknesses were obtained using a stress-based criterion that considers peel, longitudinal, transverse shear and axial stresses to approximate delamination-related failure in the adherend. Lastly, HyperX was validated against existing experimental results.

II. Verification of HyperX

A. FEA

The Abaqus finite element analysis (FEA) software was used in this work for comparison with the rapid HyperX joint analysis capability. A flat 2D composite joint, as well as two composite Y-joints with different curvatures, were modeled using plane strain CPE4 and CPE3 solid elements in a linear elastic analysis (see Fig. 2 and Fig. 3). The parts of the joint are shown in Figures 1 and 2 are follows: The tan region is an aluminum grip plate used in experiments [4] to represent an orthogonal panel, the red part is the 3D woven preform and the black part represents the vehicle fuselage skin, which is one of the joint adherends. There are explicit adhesive material layers between the preform and skin, as well as between the preform and the aluminum vertical adherend. In the model, the adhesives were assembled with the rest of the parts through tie constraints, and they have isotropic material properties (FM 300K Epoxy Film Adhesive 0.06 psf, Table 1). The preform was modeled as a homogeneous solid section, and it was given effective material properties, through engineering constants, which characterize the 3D woven material at the mesoscale (see Table 1). The skin on the other hand, was sectioned into 32 plies ($[0/\pm45/90]_{4S}$) and assigned material properties in terms of engineering constants for each of the unidirectional (UD) plies. These effective properties have

been rotated appropriately to account for the ply orientations. The composite material properties were based on AS4 fiber and RTM6 matrix constituents. All composite material properties were provided by NASA [7] and are listed in Table 1.

The joint model geometries are shown in Fig. 2 and Fig. 3. The first Y-joint has a curvature of 174.3° and the second has a curvature of 146.6°. As indicated in Fig. 2 and Fig. 3 below, the left and right boundaries of the skin are clamped, and the aluminum vertical adherend is subjected to loading upwards (in the y-direction) with a pressure of –1000 lbf/in^2. A preliminary mesh refinement study was conducted, and 714941 elements were used with 8 through-thickness elements per layer of adhesive. A complete description of the Y-joint geometry, boundary conditions, and materials can be found in [8].

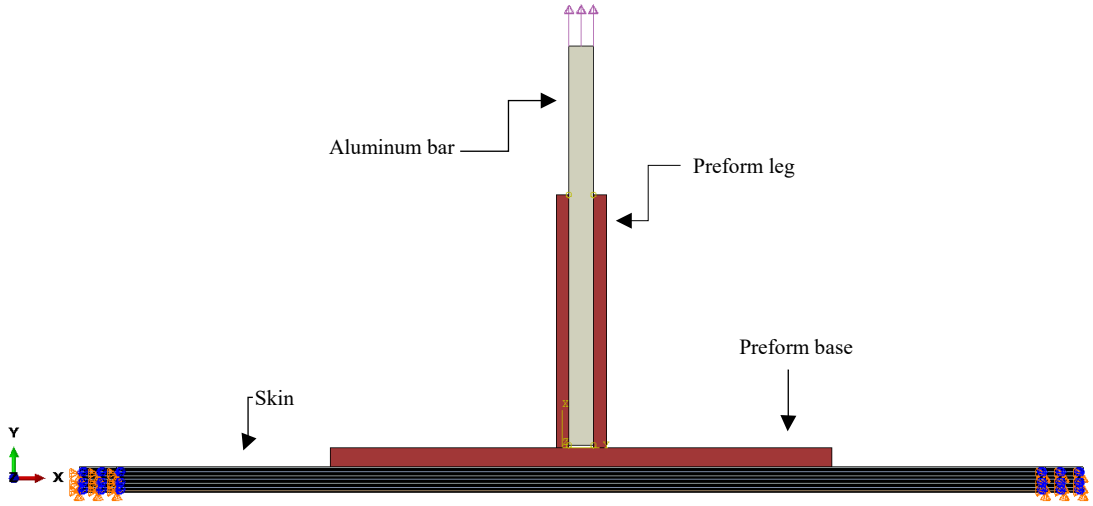

Fig. 2 Pi-joint as modeled in Abaqus, CAE.

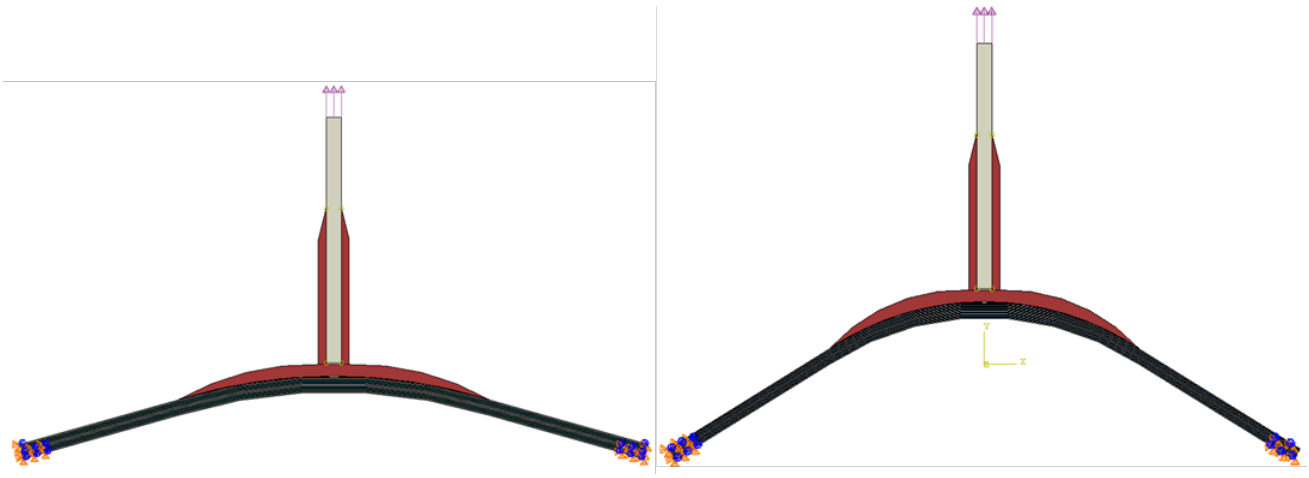

Fig. 3 Y-joint of 174.3° angle (left) and Y-joint of 146.6° angle (right) as modeled in Abaqus, CAE.

Table 1 Elastic properties for the AS4/RTM6 3D woven preform, AS4/RTM6 0° plies, Al 7075-T6 aluminum bar and FM 300K film adhesive.

	AS4/RTM6 3D Woven Preform	AS4/RTM6 0° ply	Al 7075-T6	FM 300K Epoxy Film Adhesive 0.06 psf
E_1 *(Msi)*	8.604	20.279	10.400	0.3419
E_2 *(Msi)*	8.575	0.813	10.400	0.3419
E_3 *(Msi)*	1.378	0.813	10.400	0.3419
ν_{12}	0.037	0.266	0.300	0.300
ν_{13}	0.318	0.266	0.300	0.300
ν_{23}	0.305	0.318	0.300	0.300
G_{12} *(Msi)*	0.299	0.352	4.000	0.1315
G_{13} *(Msi)*	0.297	0.352	4.000	0.1315
G_{23} *(Msi)*	0.591	0.308	4.000	0.1315

B. HyperX

HyperX is a successor software of HyperSizer [6], and it includes stress analysis and optimization of structural bonded joints. This stress analysis is based on Mortensen's unified approach [9], [10], and it has been further developed further to calculate the through-thickness (interlaminar) peel and shear stresses arising locally in the adherends [11] - [13]. The HyperX software can consider the joint configurations shown in Fig. 4. To analyze an equivalent to the two joints presented in this work (Pi-joints and Y-joints), a combination of two joint configurations available in HyperX were used. Fig. 5 shows the regions in the joints that were analyzed in HyperX as two different joint configurations. Region 1 was modeled as a bonded clevis, while region 2 was modeled as a bonded doubler. Dividing the continuous Pi- and Y-joints in this manner neglects interactions of the stress concentrations that arise locally in the two, now completely separated, bonded joints. This constitutes one potential source of discrepancy between the FEA and HyperX analyses.

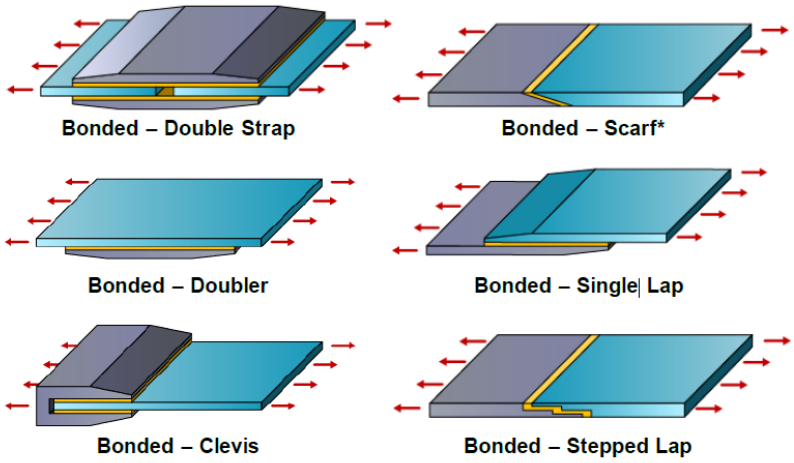

Fig. 4 Joint configurations supported by HyperX [12].

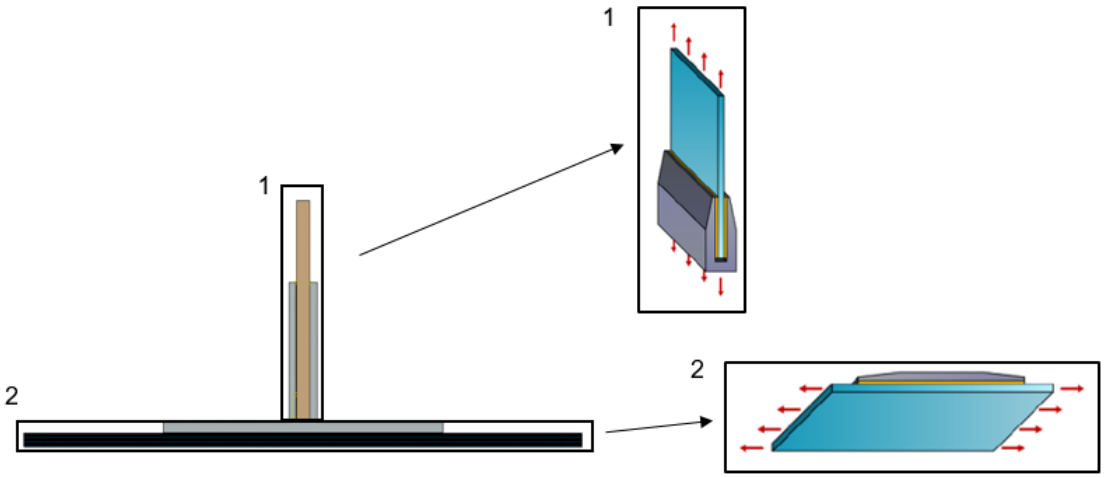

Fig. 5 Regions in the Abaqus model that have been analyzed as two separate joints in HyperX (region 1: bonded clevis, region 2: bonded doubler).

The boundary conditions that are applied to the two individual HyperX joint concepts (clevis and doubler) are critical and must be defined appropriately to capture the correct mechanics of an effective Pi-joint or Y-joint. Starting with the Pi-joint, the boundary conditions for each of the joints that are intended to simulate a pull-off test, are shown in Fig. 6 and Fig. 7. For the bonded clevis, a force resultant of N_y = 192 lbf/in was applied to the adherend (aluminum bar), at location 1 in Fig. 6, which equates to a stress value of 1000 lbf/in^2 when factoring the bar thickness. The end of the clevis (boundary conditions at locations 2 and 3) was held fixed (displacements are equal to zero). Locations 4, 5, and 6 were not restrained. In HyperX, half of the bonded doubler joint is modeled using symmetry, and it is shown in Fig. 7. Hence, a transverse (shear) force resultant of Q_y = 98 lbf /in was used in location 3 to load the doubler. At location 1, the doubler is restricted in axial, transverse, moment, and shear, while at location 4, the doubler is left unrestrained. Finally, in location 2, the doubler axial and transverse displacements were restrained. Table 2 and Table 3 show the boundary conditions as entered in HyperX.

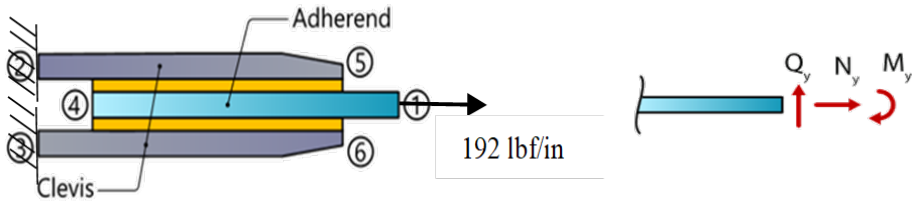

Table 2 Boundary conditions for the Pi-joint clevis.

Location	Axial	Transverse	Moment	Shear
1	$N_y = 192$ lbf/in	w = 0 in	β = 0 rad	u = 0 in
2	Fixed	Fixed	Fixed	Free
3	Fixed	Fixed	Fixed	Free
4	Free	Free	Free	Free
5	Free	Free	Free	Free
6	Free	Free	Free	Free

Fig. 6 Sign conventions and boundary conditions of bonded clevis of the Pi joint in HyperX.

Table 3 Boundary conditions for the Pi-joint doubler.

Location	Axial	Transverse	Moment	Shear
1	Fixed	Fixed	Fixed	Fixed
2	Fixed	Fixed	Free	Free
3	Fixed	$Q_y = 96$ lbf/in	Fixed	Free
4	Free	Free	Free	Free

Fig. 7 Sign conventions and boundary conditions of bonded doubler of the Pi-joint in HyperX.

Regarding the Y-joint model, first, the bonded clevis region does not differ in geometry or boundary conditions from the Pi-joint model. For the Y-joint doubler region, even though the point-wise curvature of the adherends is relatively mild, the loads are transferred differently due to a large-scale shape difference compared to the flat geometry. To account for the first-order effects of the curvature, it has been assumed that the joint stress fields will depend mainly on the eccentricity of the load path, as opposed to the local curvature. The curvature in the preform base and the skin of the Y-joint was thus accounted for through boundary conditions in location 3 on the bonded doubler. Note that this is an engineering approximation enabling the existing HyperX flat joint capabilities to be applied to the curved Y-joint. The impact of this approximation will be evaluated below through the comparison to FEA results. The 96 lbf/in transverse force resultant on the Y-joint was decomposed into its components (axial force, transverse force, and moment) in the HyperX doubler. As stated previously, HyperX runs the analysis for half of the doubler and thus half of the transverse force resultant (192 lbf/in) was applied to the doubler. Fig. 8 shows the decomposition of the force into its components. The Y-joint shown for example has an angle of curvature of 146.6° and the angle between the two coordinate systems was calculated to be $16.7°((180° - 146.6°)/2 = 33.4°/2)$. The employed boundary conditions of the Y-joint are shown, for the 146.6° example, in Fig. 9.

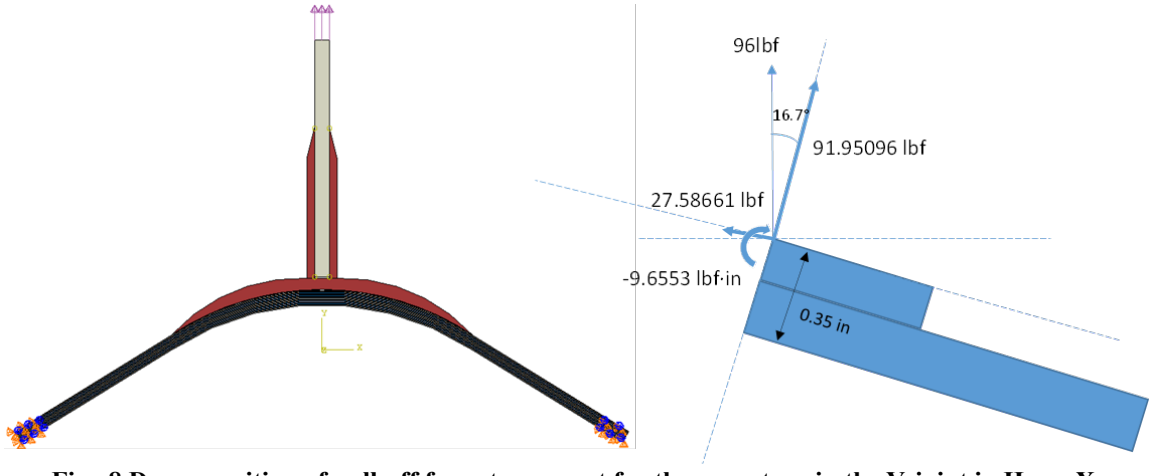

Fig. 8 Decomposition of pull-off force to account for the curvature in the Y-joint in HyperX.

Table 4 Boundary conditions for the Y-joint doubler.

Location	Axial	Transverse	Moment	Shear
1	Fixed	Fixed	Fixed	Fixed
2	Fixed	Free	Free	Free
3	$N_y = 27.59$ lbf/in	$Q_y = 91.95$ lbf/in	$M_y = -9.655$ lbf · in	Free
4	Free	Free	Free	Free

Fig. 9 Sign convention and boundary conditions of bonded doubler for Y-joint in HyperX.

The material properties used in HyperX were the same as the material properties used for the Abaqus analysis (Table 1). In HyperX, the laminated skin as well as the preform were modeled as laminates. Thus, for the preform, a laminate was defined with thickness equal to the preform base thickness and the effective material properties of the 3D woven composite (Table 1). The skin in all HyperX models consisted of 32 unidirectional plies (0.00625 in ply thickness) with quasi-isotropic laminate stacking sequence ($[0/\pm45/90]_{4S}$).

C. Verification Results

To compare the joint stress analysis prediction between Abaqus and HyperX, the peel and shear stresses along the adhesives have been compared. While this does not give a complete assessment of all stress components throughout the joints, it is quite representative as the load path is through the adhesive for the loading considered and the prominent bonded joint and re-entrant corner stress concentrations are typically in the vicinity of the adhesive. This is partly because the adhesive peel and shear stresses are tractions, and thus must be continuous in the through-thickness direction from one adherend, into the adhesive, and into the other adherend. For the clevis region, only one of the adhesives between the preform leg and the aluminum bar has been considered (results for the other adhesive are identical). For the doubler region, the stresses in half of the adhesive between the preform base and the skin have been reported. According to experimental tests from Aurora Flight Sciences [4], the Y-joint consistently failed in the joint center region close to the preform-to-skin interface. Thus, this study places emphasis on this region, where the failure was observed. All stresses shown in this section are plotted vs. the distance along the adhesive path. Fig. 10 shows the starting points (x = 0) of the adhesive path for the clevis (left) and the adhesive path for the doubler (right). It should be noted that the path for the doubler starts under the preform upright (right-side in Fig. 10). The flat Pi joint is shown for simplicity in Fig. 10, but analogous paths are followed for the Y-joints.

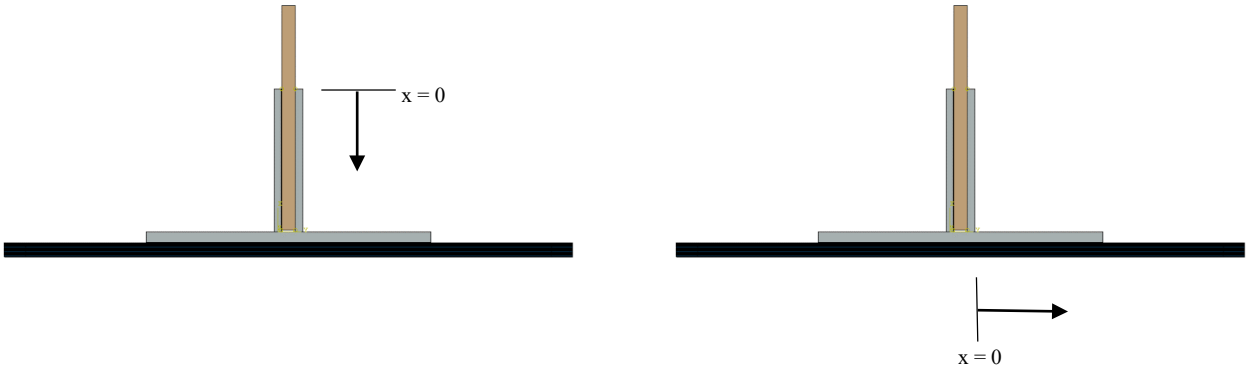

Fig. 10 Path along the adhesive for clevis region (left) and doubler region (right).

Fig. 11 shows the peel and shear stresses in the adhesive of the clevis region of the Pi joint. As seen, the clevis configuration in HyperX agrees quite well with Abaqus until the region close to the preform base is reached (right side of plots in Fig. 11). The boundary conditions and shell formulation in HyperX cannot account for the 3D effects in this region. In addition, the employed FEA model maintains a thin open gap between the aluminum bar and the base of the Pi preform. In practice, gap filler material is often used in this region. However, since the region of

interest is part of the bonded doubler joint configuration, the bonded doubler is the focus of the study and will be used for the remained of the analyses and comparisons for all Y-joints studied.

The peel and shear stresses in the adhesive of the bonded doubler of the Pi joint are shown in Fig. 12. As mentioned, only half of the doubler is considered and due to symmetry; the results are symmetric for the other half of the doubler. It should be noted that the path of the adhesive starts under the end of the preform leg (see Fig. 10) because the force is transferred through the preform legs, and the boundary conditions in HyperX were chosen to mimic this location's force transfer. The adhesive stresses for the flat Pi joint in HyperX are in good agreement with Abaqus. Most importantly, the shapes of the curves are similar, meaning the first-order characteristics of the joint are well captured in HyperX. The "trough" in the peel stress (stress decrease before the high concentration on the right side of the plot) is overpredicted by HyperX compared to FEA, but this is a known effect of the shell model used in HyperX [13]. This area towards the end of the adhesive (right edge of Fig. 10) is not the primary area of interest (it is not where the failure is typically observed). As mentioned, the differences in this area are typical between shell-based and continuum based joint models [14].

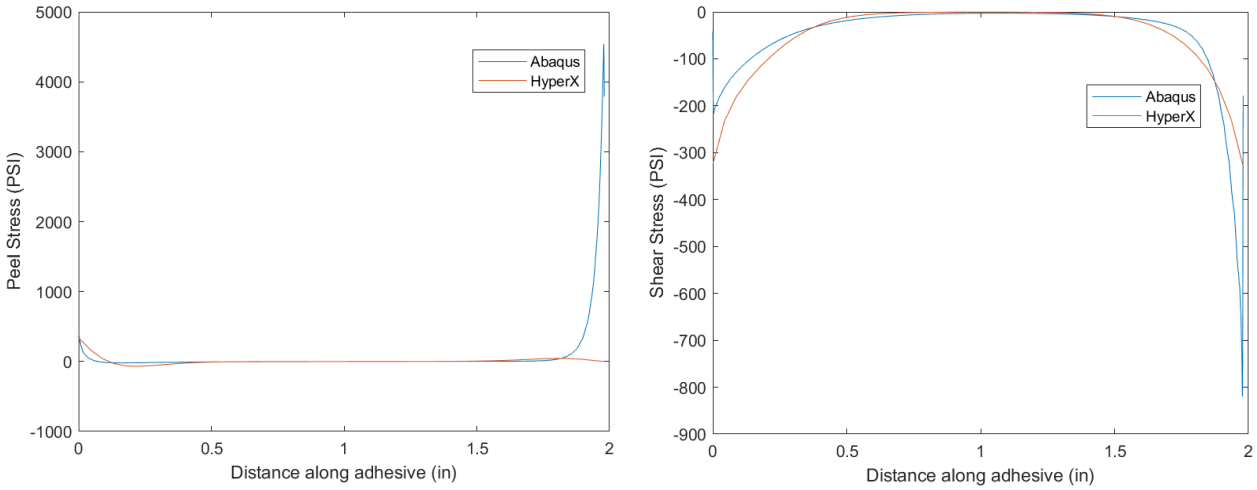

Fig. 11 Peel stress (left) and shear stress (right) along the adhesive of the clevis of the Pi-joint in Abaqus and HyperX.

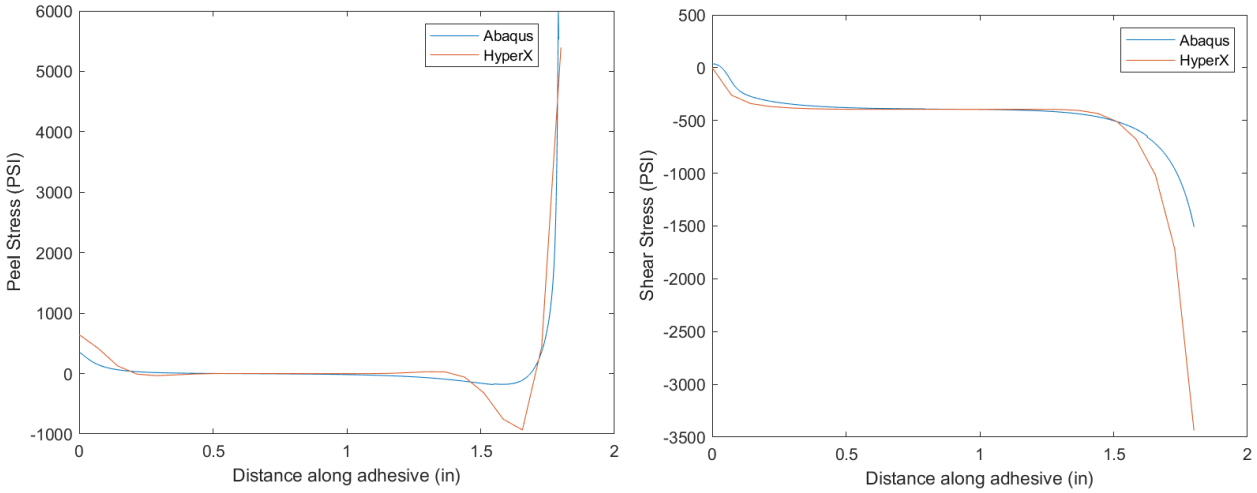

Fig. 12 Peel stress (left) and shear stress (right) along the adhesive of the doubler of the Pi-joint in Abaqus and HyperX.

Fig. 13 shows the peel and shear stresses in the adhesive of the bonded doubler in the Y-joint. Despite decent qualitative agreement between HyperX and Abaqus, it is evident that the curvature in the joint results in more differences in the stress results between the two analysis methods. HyperX tends to overpredict the magnitudes of both the peel and shear stresses in the region of interest. However, the good qualitative agreement indicates that HyperX can readily be used for design through appropriate correlation with experimental joint strength data. Note that the path of the adhesive shown in the plots stops at 1.05 in. After 1.1 in into the adhesive path, the HyperX results exhibit some oscillations that indicate additional points are required in the x-direction due to the ply drops in this region.

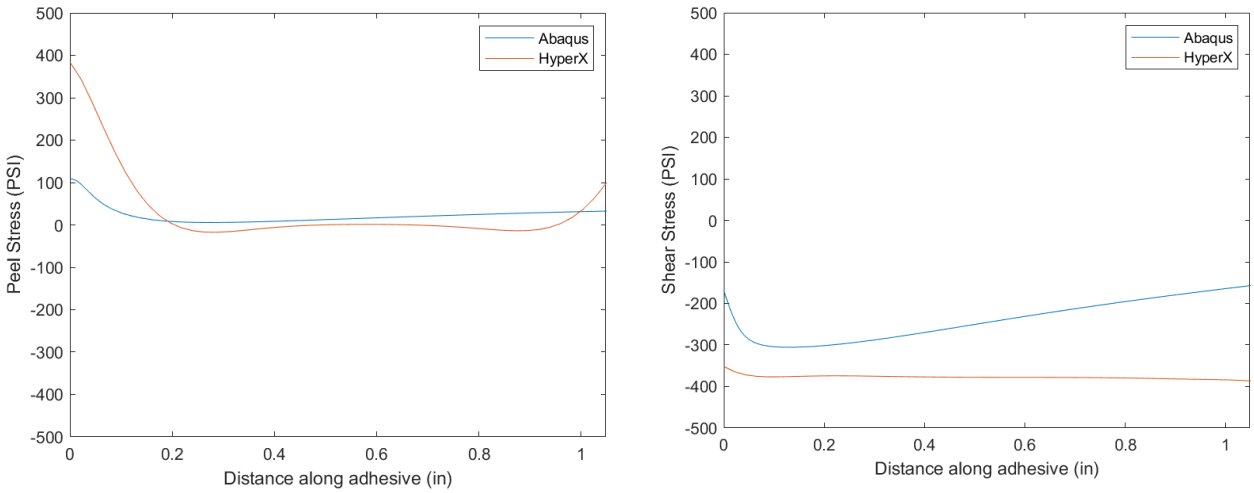

Fig. 13 Peel stress (left) and shear stress (right) along the adhesive of the doubler of the Y-joint in Abaqus and HyperX.

III. Parametric Studies

Parametric studies can reveal crucial sensitivities that can guide the design and optimization process. In this study, four major parametric studies were completed using HyperX. The parameters explored were the curvature of the joint, the thickness of laminated skin and the material system of the adhesive. The HyperX results shown in this section consider the adhesive in the bonded doubler starting below right-side upright preform leg and until the tapered region (approximately 1.2 in). While that is a subject for further future development, in the current work, it has not been considered vital as the focus is the region of the doubler under the clevis.

A. Curvature Parametric Study

Three different curvatures were studied: 174°, 165°, and 147°, with the curvature angle as shown in Fig. 3. HyperX results showing the sensitivity of the Y-joint adhesive stresses to joint curvature are plotted in Fig. 14. As seen, the trends in both peel and shear stresses in the adhesive are consistent. As the curvature of the joint increases, both the peel and the shear stresses decrease in magnitude. Most notably, as the joint curvature is increased, the peel stress at the center of the joint (beneath the clevis) changes from tensile to compressive, while the slope of the shear stress switches signs. However, for all three curvatures, there remains a significant tensile peel stress peak (which decreases with curvature). This would have a significant impact on the joint performance as this is exactly where Y-joint failure has been observed in experiments (see Fig. 1).

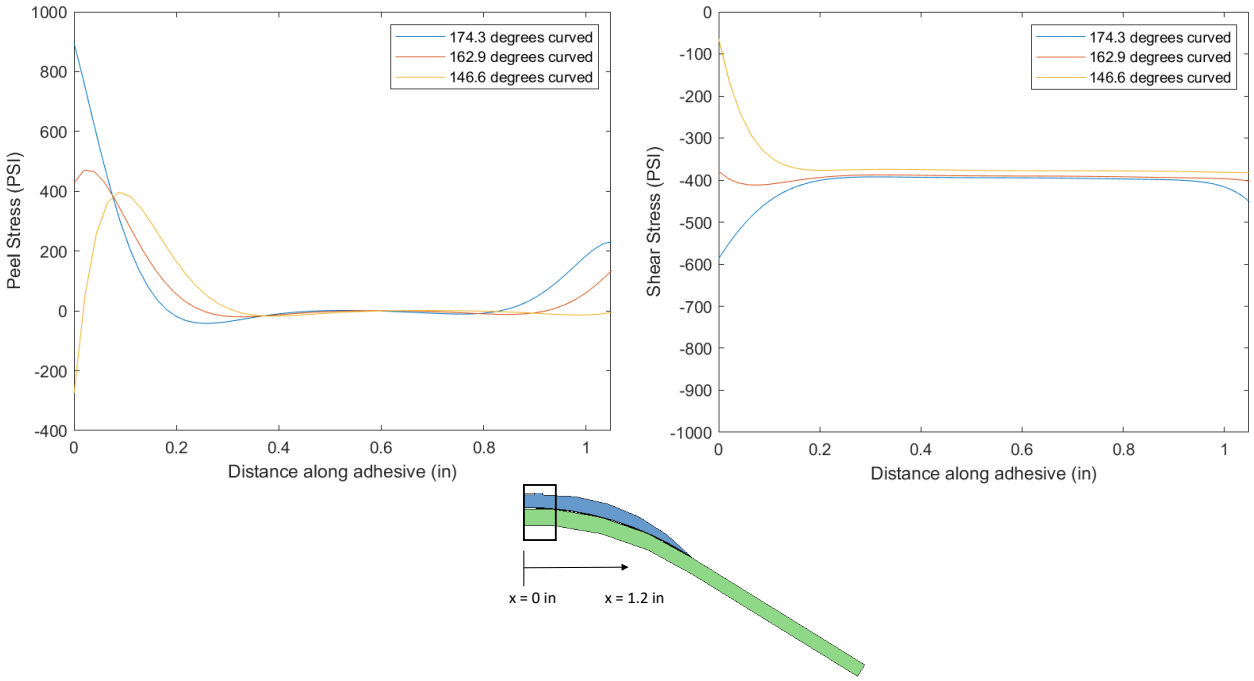

Fig. 14 Peel stress (left) and shear stress (right) along the adhesive of the doubler for Y-joints of different curvatures in HyperX.

B. Skin Thickness

The effects of thick and thin laminated skins were investigated by considering a 16 ply skin, 24 ply skin, and 32 ply skin. The laminate layup was always $[0/45/-45/90]_{nS}$ with a ply thickness of 0.00625 inches. The material properties are the same as the ones used throughout the HyperX verification process (given in Table 1).

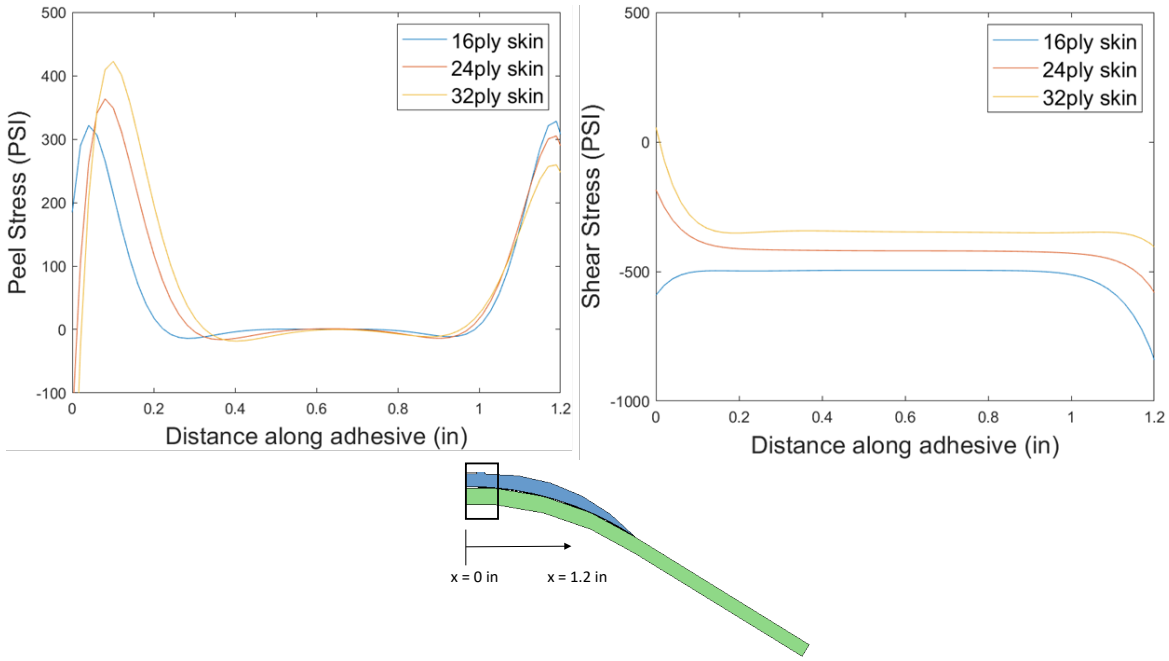

Fig. 15 Peel stress (left) and shear stress (right) along the adhesive of the doubler for Y-joints with different skin thicknesses in HyperX.

The effect on the peel and shear stresses in the adhesive when changing the laminated skin thickness are shown in Fig. 15. As the skin gets thicker, the peak peel stresses increase. The peak shear stresses decrease in magnitude when the skin thickness increases. Another interesting observation is that with thicker skin the peak peel stresses located close to the area of interest (left side of the plots in Fig. 15) become higher in magnitude than the peak stresses close to the tapered doubler (right side of the plots in Fig. 15).

C. Adhesive Systems

Two kinds of adhesive systems were investigated: film adhesives and paste adhesives. Four commonly used in aerospace adhesives were considered, two of which are film adhesives (Grade 5 FM300, FM300K) and the other two are paste adhesives (Unisorb V-100, Hysol 9394). Material properties for Unisorb V-100, EA Hysol 9394, and Grade 5 FM300 were found in the literature [15], [12], and [16] respectively, while FM 300K Epoxy Film Adhesive, 0.006 psf, is a default material in the HyperX software. All material properties are given in Table 5.

Table 5 Material properties and thicknesses for the film adhesives and paste adhesives.

	Unisorb V-100	EA Hysol 9394	Grade 5 FM 300	FM 300K Epoxy
Thickness t_a (in)	0.05	0.025	0.007	0.004
E_a (Msi)	0.436	0.456	0.2495	0.3419
v	0.35	0.3	0.3	0.3
G_a (Msi)	0.161481	0.175385	0.09596	0.1315
E_a / t_a (Msi/in)	8.72	18.24	35.64286	85.475
G_a / t_a (Msi/in)	3.22963	7.015385	13.70879	32.875

Results from HyperX for the sensitivity study on the effect of adhesive systems on the Y-joint are shown in Fig. 16. As observed, the peel and shear peak stresses under the clevis part of the doubler increased in magnitude as the ratio of adhesive modulus to thickness becomes larger. It should be noted that the ratio of modulus to thickness should be considered for this study as the constitutive relationship used in HyperX for the adhesive layer is a linear spring adhesive model with peel and shear stress equations [13]:

$$\sigma_a = \frac{E_a}{t_a}\left(w^i - w^j\right) \tag{1}$$

$$\tau_{ax} = \frac{G_a}{t_a}\left(u^i - u^j\right) \tag{2}$$

where i, j are the adherend numbers, E_a, G_a, and t_a are the adhesive Young's modulus, shear modulus, and thickness, respectively, and w, u are the adherend through-thickness and axial midplane displacements, respectively.

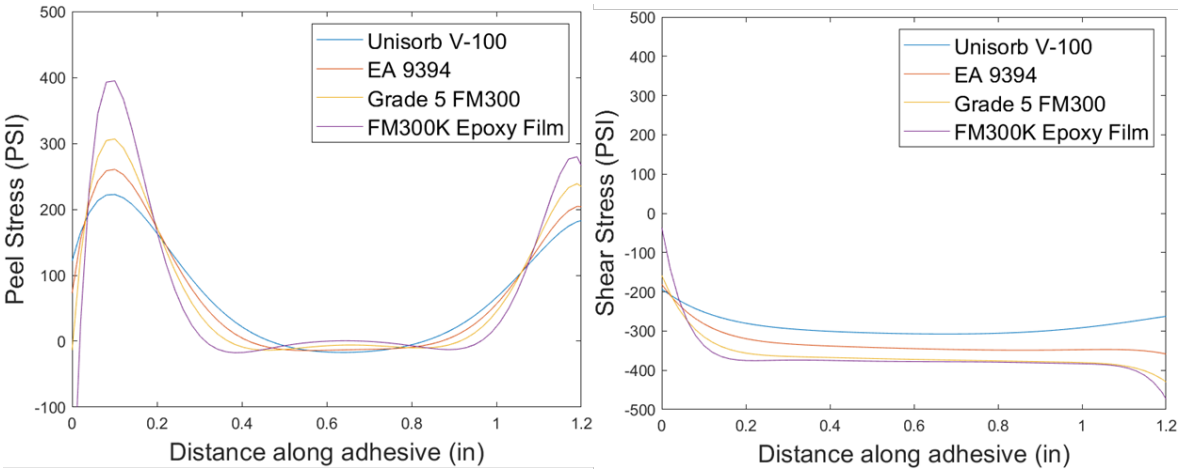

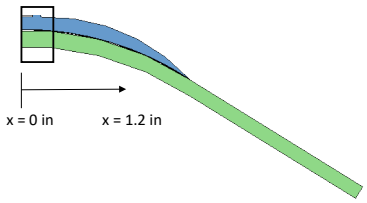

Fig. 16 Peel stress (left) and shear stress (right) along the adhesive of the doubler for Y-joints with different adhesive systems in HyperX.

D. Failure Load Predictions

HyperX was used to investigate some trends in the predicted failure load of the doubler configuration as the Y-joint curvature and the thickness of the laminated skin were altered. Failure prediction capabilities have been developed in HyperSizer and passed on to HyperX for the joint configurations currently supported [16], [17]. An initial investigation into the failure load prediction capability of HyperX for the Y-joint was done by Plaka et al. [8] and it was concluded that, of the stress-based failure criteria available in HyperX, interactive failure criteria are best for the present application. Throughout the failure predictions analysis, the adhesive material did not show failure and thus failure predictions according to adhesive failure criteria are not reported. The failure loads were determined according to the HyperX stress-based failure criterion suggested by Tong [11]:

Delamination, Tong, Peel, Transverse Shear & Axial 4

$$\left(\frac{\sigma_1}{F_1^{tu}}\right)^2+\left(\frac{\sigma_3}{F_3^{tu}}\right)+\left(\frac{\tau_{13}}{F_{13}^{su}}\right)^2=1 \qquad (3)$$

where F_1^{tu}, F_3^{tu}, and F_{13}^{su} are the ultimate normal stress allowable in the 1 direction, the ultimate normal stress allowable in the 3 direction, and the out-of-plane shear stress allowable in 13 ply coordinates respectively; and σ_1, σ_3, and τ_{13} are the normal stress in 1 direction, normal stress in 3 direction, and shear stress in 13 ply coordinates respectively.

The laminated skin thickness of the Y-joint with an angle of curvature of 146.6° was varied between 0.1 inches and 0.2 inches. Adhesive nonlinear material behavior was included, which has been shown to be more accurate than linear-elastic properties due to the relative ductility of aerospace adhesives [9]. The strength allowables for the skin, preform, and adhesive are given in Table 6 and Table 7. The skin strength allowables are notional. Since the purpose of this effort is to show that HyperX can be used to predict failure trends and not to quantify any joint analysis at this stage, notional values are acceptable. The adhesive allowables are provided as an example material in HyperX, while the 3D woven strength values are taken from the literature [18]. It should be noted that all compressive properties are assumed to be the same as the tensile property values.

Table 6 Strength values for the AS4/RTM6 3D woven preform material, AS4/RTM6 laminated skin material.

	AS4/RTM6 3D Woven Preform	AS4/RTM6 0° ply
Longitudinal Strength F_1^{tu}*(ksi)*	117.5	294.8
Transverse Strength F_2^{tu} *(ksi)*	119.1	34.71
In-plane shear strength F_{12}^{su} *(ksi)*	5.802	16.13
Through-thickness Strength F_3^{tu} *(ksi)*	10.2	4.863
Interlaminar shear strength F_{13}^{su} *(ksi)*	6.121	9.78
Interlaminar shear strength F_{23}^{su} *(ksi)*	5.845	5.379

Table 7 Elastic material properties and strengths for FM 300K Epoxy film Adhesive 0.06psf.

	E^t (Msi)	E^c (Msi)	G (Msi)	ν^t	ν^c	n	$F0.2$ (ksi)	F_{peel}^{adh} (ksi)	F_{shear}^{adh} (ksi)
FM 300K 0.06psf	0.3419	0.3419	0.1315	0.3	0.3	11.3	4.5	11.02	5.51

Results for the failure load predictions for varying Y-joint curvature and skin thickness are shown in Fig. 17 and Fig. 18 respectively. Local stresses are taken from the region of the doubler between x = 0 in and x = 0.8 in (see Fig. 10), to avoid the evaluation of oscillating stresses at the end of the doubler region (discussed above) in the calculation of margins of safety. HyperX evaluates failure criteria at all points in the considered regions of the joint, and the failure load has been evaluated as the lowest load that first causes the failure criterion (Eq. 3) to be exceeded at some point in the joint. As seen in Fig. 17, HyperX predicts that the failure load increases with an increased curvature in the Y-joint. In future work, additional curvatures will be explored. From Fig. 18 it is evident that the failure load increases with a decrease in the skin thickness. This result may seem somewhat counterintuitive as a thicker, heavier skin is leading to a lower strength joint. However, it is the local stress concentrations predicted in the joint analysis that leads to the failure criterion being exceeded. Further, as the skin becomes thicker, the mismatch between the skin and doubler structural stiffness increases, which leads to higher stress concentrations (see Fig. 16). It should be mentioned again that the trends in the failure load predictions are of primary interest here, as opposed to the predicted failure loads magnitudes. It should also be noted that HyperX includes the Virtual Crack Closure Technique (VCCT) [12], [19] for energy-based failure predictions of joints containing an existing flaw. Future work is planned to apply this capability to the Y-joint using mode-specific critical strain energy release rates, rather than stress allowables, to characterize the failure of the adherend materials.

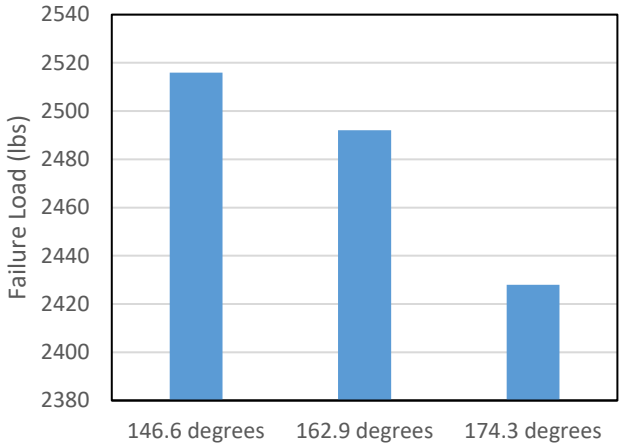

Fig. 17 Failure load prediction in HyperX for varying Y-joint curvature using the Tong 4 failure criterion, Eq. 3.

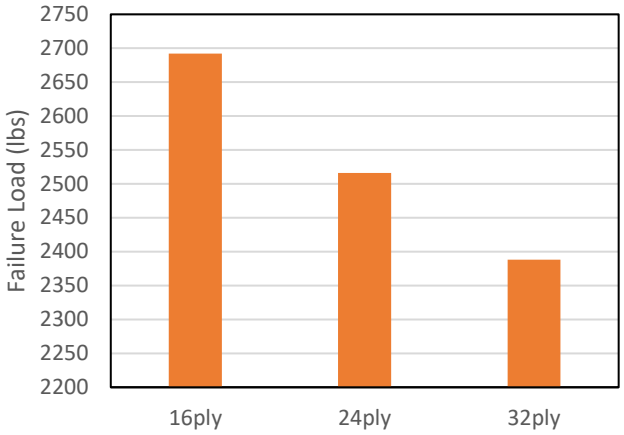

Fig. 18 Failure load prediction in HyperX for varying skin thickness using the Tong 4 failure criterion, Eq. 3.

IV. Validation of HyperX

The implementation of the Y-joint in HyperX for the purposes of this work was also validated vs. experimental data. Since no experimental data for the AS4/RTM6 material system considered above exists, the material used for the validation process was switched to T800/3900, and the HyperX model was validated against Aurora's experiments on the Y-joint baseline configuration [4]. Using dimensions for the Y-joint reconstructed by images of the joint from Aurora in [4], and two layers of film adhesive, HyperX was used to predict the failure pull-off load of the Y-joint. The composite preform was a 3D weave, while the skin was made of laminates in a $[0/45/-45/90]_{3S}$ stacking sequence. The adhesive used was FM300M 0.03 psf film adhesive. The elastic material properties and strength allowables used for the skin and preform of the Y-joint are shown in Table 8, while the material properties used for the adhesive material are given in Table 9.

Table 8 Elastic material properties and stress allowable for T800/3900 plies and 3D weave.

	T800/3900 Ply (0°)	T800/3900 3D Weave
E_1^t (Msi)	21.5	10
E_2^t (Msi)	1.24	9.86
ν_{12}^t	0.332	0.032
E_1^c (Msi)	18.9	9.23
E_2^c (Msi)	1.23	8.92
ν_{12}^c	0.339	0.044
G_{12} (Msi)	0.571	0.521
G_{13} (Msi)	0.571	0.306
G_{23} (Msi)	0.422	0.306
F_1^{tu} (ksi)	436	150
F_2^{tu} (ksi)	8.93	134
F_1^{cu} (ksi)	258	96.9
F_2^{cu} (ksi)	31.3	87.5
F_{12}^{su} (ksi)	10.1	11.5
F_{13}^{su} (ksi)	10.1	10.8
F_{23}^{su} (ksi)	5.611	10.16
F_3^{tu} (ksi)	8.72	13.02

Table 9 Elastic material properties and stress allowables for FM300M 0.03 psf film adhesive.

	E^t (Msi)	E^c (Msi)	G (Msi)	ν^t	ν^c	n	$F0.2$ (ksi)	F_{peel}^{adh} (ksi)	F_{shear}^{adh} (ksi)
FM300M 0.03psf	0.299	0.299	0.115	0.3	0.3	17.1	4.362	11.432	5.716

Using two different stress-based interactive failure criteria for the adherends, two different failure loads were predicted, which gave an upper and a lower failure load bounds when compared to the experimental data. The failure criteria used are characterized by the equation (3) and equation (4) given below:

Delamination, Tong, Peel, Transverse Shear & Axial 3

$$\left(\frac{\sigma_1}{F_1^{tu}}\right)^2+\left(\frac{\sigma_3}{F_3^{tu}}\right)^2+\left(\frac{\tau_{13}}{F_{13}^{su}}\right)^2=1 \qquad (4)$$

Note that the only difference between Eqs. (3) and (4) is the exponent on the peel stress (σ_3) term.

The two failure loads predicted by HyperX were 4328 lbs and 3884 lbs according to Tong, Peel, Transverse Shear & Axial 3 and 4 respectively. The experimental results showed an average ultimate failure load of 4239 lbs. The HyperX predicted failure loads bound the Aurora's average experimental results [4], and they are both within 10%. This indicates that HyperX, is capable of accurately predicting failure loads for a curved Y-joint. This result

coupled with the code's ability to predict realistic trends indicate the utility of HyperX for optimizing composite Y-joints.

V. Conclusions

The results reported herein indicate that the rapid joint design tool software of choice (HyperX) can be used for the analysis and optimization of the Y-joint. Good agreement between the HyperX and Abaqus models in the region of interest has been shown. Additionally, HyperX can be used to explore the trends in the stress predictions through sensitivity studies. This has been shown through three parametric studies performed: curvature, skin thickness, and adhesive material system parametric studies. The curvature and skin thickness in the Y-joint showed the most significant impact on the stress distribution and were chosen to investigate the prediction of failure loads in the joint based on existing stress-based failure criteria. HyperX predicted consistent and realistic trends in failure loads with varying curvature and skin thickness. Further, more in depth study will be performed in the prediction of failure loads and the determination of appropriate failure criteria, including the use of the HyperX VCCT capability. Lastly, as described in the Validation section of the paper, HyperX was used to predict the failure load of one of the Y-joint configurations tested by Aurora Flight Sciences (again, using stress-based failure criteria) and was shown to be within 10% of the average measured value.

VI. References

[1] Behera, B.K., and B.P. Dash. "Mechanical Behavior of 3D Woven Composites." *Materials & Design* 67 (February 2015): 261–71. https://doi.org/10.1016/j.matdes.2014.11.020.

[2] Gerlach, R., Siviour, C.R., Wiegand, J., and Petrinic, N. "In-Plane and through-Thickness Properties, Failure Modes, Damage and Delamination in 3D Woven Carbon Fibre Composites Subjected to Impact Loading." *Composites Science and Technology* 72, no. 3 (February 2012): 397–411. https://doi.org/10.1016/j.compscitech.2011.11.032.

[3] Chambers, J.T., Oonnoonny, A., Yutko, B.M., and Church, C.S., "3-D Woven Preform Joint Testing to Support the D8 Double-Bubble Composite Fuselage Design," Proc. American Society for Composites—Thirty-second Technical Conference, October 23-25, 2017.

[4] Chambers, J.T., Yutko, B.M., Oonnoonny, A., Hoffman, D.R., and Church, C.S., "3-D Woven Preform Joint Experimental Testing Results to Support the D8 Double-Bubble Composite Fuselage Design," in AIAA/ASCE/AHS/ASC Structures, Structural Dynamics, and Materials Conference, January 8-12, 2018.

[5] Chambers, J.T., Yutko, B.M., Singh, R.C., and Church, C.S., "Structural Optimization Study of the D8 Doubler-Bubble Composite Fuselage," in 58th AIAA/ASCE/AHS/ASC Structures, Structural Dynamics, and Materials Conference, January 9-13, 2017.

[6] HyperSizer. Available from: https://hypersizer.com/hyperx/.

[7] Pineda, E.J., Bednarcyk, B.A., and Ricks, T.M. "Multiscale Progressive Failure Predictions for 3D Woven Composites," n.d., 10.

[8] Plaka, E., *Optimization of the D8 Double Bubble Composite Y-Joint,* in *Department od Mechanical Engineering.* 2021, University of Massachusetts Lowell.

[9] Mortensen, F., and Thomsen, O.T. "Coupling Effects in Adhesive Bonded Joints." Composite Structures 56, no. 2 (January 1, 2002): l165–74. doi:10.1016/S0263-8223(02)00002-8.

[10] Mortensen, F., and Thomsen, O.T. "Analysis of Adhesive Bonded Joints: A Unified Approach," Composites Science and Technology, vol. 62, no. 7, pp. 1011-1031, 2002.

[11] "HyperSizer Bonded Joint User Manual." Newport News, VA: Collier Research Corporation, 2019.

[12] Jones, S.P., Stier, B., Bednarcyk, B.A., Pineda, E.J., and Palliyaguru, U.R., "Verification, Validation, and Limits of Applicability of a Rapid Bonded Joint Analysis Tool," in AIAA SciTech 2020 Forum, January 6-10, 2020.

[13] Zhang, J., Bednarcyk, B.A., Collier, C., Yarrington, P., Bansal, Y., and Pindera, M-J., "3D Stress Analysis of Adhesive Bonded Composite Joints," in 46th AIAA/ASCE/AHS/ASC Structures, Structural Dynamics, and Materials Conference, April 18-21, 2005.

[14] Stapleton, S.E., Stier, B., Jones, S.P., Bergan, A., Kaleel, I., Petrolo, M., Carrera E., and Bednarcyk, B.A., "A critical assessment of design tools for stress analysis of adhesively bonded double lap joints," in Mechanics of Advanced Materials and Structures, June 19, 2019, DOI: 10.1080/15376494.2019.1600768.

[15] Pineda, E.J., Myers, D.E., Kosareo, D.N., Zalewski, B., Kellas, S., Dixon, G.D., Krivanek, T.M., and Gyekenyesi, T.G. "Buckling Testing and Analysis of Honeycomb Sandwich Panel Arc Segments of a Full-Scale Fairing

Barrel: Comparison of In- and Out-of-Autoclave Facesheet Configurations." *55th AIAA/ASME/ASCE/AHS/ASC Structures, Structural Dynamics, and Materials Conference*. National Harbor, Maryland: American Institute of Aeronautics and Astronautics, 2014. https://doi.org/10.2514/6.2014-1052.

[16] Yarrington, P., Zhang, J., Collier, C., and Bednarcyk, B. "Failure Analysis of Adhesively Bonded Composite Joints." In 46th AIAA/ASME/ASCE/AHS/ASC Structures, Structural Dynamics and Materials Conference. Austin, Texas: American Institute of Aeronautics and Astronautics, 2005. https://doi.org/10.2514/6.2005-2376.

[17] Yarrington, P., Collier, C., and Bednarcyk, B. "Failure Analysis of Adhesively Bonded Composite Joints via the Virtual Crack Closure Technique," AIAA 2006-1962. *47th AIAA/ASME/ASCE/AHS/ASC Structures, Structural Dynamics, and Materials Conference*. May 2006. https://doi.org/10.2514/6.2006-1962.

[18] Pineda, E.J., Bednarcyk, B.A., Ricks, T.M., Arnold, S.M., and Henson, G., "Efficient Multiscale Recursive Micromechanics of Composites for Engineering Applicaitons," *International Journal for Multiscale Computational Engineering*, Vol. 19, 2021, pp. 77-105.

[19] Krueger, R. "The Virtual Crack Closure Technique: History, Approach and Applications," no. 2002 (2002): 64. NASA/CR-2002-211628. ICASE Report No. 2002-10.